Room-temperature magnetic bistability in organic radical crystals: Paramagnetic-diamagnetic phase transition in 1,3,5-trithia-2,4,6-triazapentalenyl

Wataru Fujita
Department of Basic Science, Graduate School of Arts and Sciences, The University of Tokyo, Komaba, Meguro-ku, Tokyo 153-8902, Japan

Kunio Awaga
Department of Basic Science, Graduate School of Arts and Sciences, The University of Tokyo, Komaba, Meguro-ku, Tokyo 153-8902, Japan
and PRESTO, Japan Science and Technology Corporation, Kudan-Minami, Tokyo 102-0074, Japan

Hiroyuki Matsuzaki
Department of Advanced Materials Science, Graduate School of Frontier Sciences, The University of Tokyo, Tokyo 113-8656, Japan

Hiroshi Okamoto
Department of Advanced Materials Science, Graduate School of Frontier Sciences, The University of Tokyo, Tokyo 113-8656, Japan
and PRESTO, Japan Science and Technology Corporation, Kudan-Minami, Tokyo 102-0074, Japan

(Received 29 November 2000; revised manuscript received 21 June 2001; published 23 January 2002)

An organic radical, 1,3,5-trithia-2,4,6-triazapentalenyl (TTTA), exhibits a first-order phase transition between a paramagnetic high-temperature (HT) phase and a diamagnetic low-temperature (LT) phase, with a surprisingly wide thermal hysteresis loop over the temperature range 230–305 K. The crystal structure of the HT phase consists of a one-dimensional (1D) regular π-stacking column with short S···N and S···S intercolumn contacts. The intra- and intercolumn exchange coupling constants are estimated to be $J/k_B = -320$ K and $zJ'/k_B = -360$ K, indicating a 3D magnetic interaction. The LT phase has a diamagnetic property, caused by a strong alternation in the stacking column. The differential scanning calorimetry measurements reveal an exothermic and an endothermic transition upon cooling and heating, respectively, with the hysteresis in agreement with static magnetic measurements. The observed transition entropy is larger than the maximum estimation of the spin contribution, $R \ln 2$, suggesting incorporation of the lattice system in this phase transition. The electron paramagnetic resonance measurements also demonstrate the paramagnetic-diamagnetic phase transition with the hysteresis. The reflection spectra suggest a change in dimensionality at the phase transition, which is consistent with the results of the intermolecular overlap-integral calculations.

DOI: 10.1103/PhysRevB.65.064434 PACS number(s): 75.50.Xx, 75.20.−g

I. INTRODUCTION

The magnetic properties of molecule-based materials have been extensively studied.[1] It is characteristic that these materials often exhibit paramagnetic-diamagnetic phase transitions, reflecting strong spin-lattice interactions in them. Many Fe(II) complexes with the ligands of intermediate crystal-field intensities make the so-called spin crossover transitions between the high ($S=2$) and the low ($S=0$) spin state.[2] Some specific organic radicals with quasi-one-dimensional (quasi-1D) crystal structures, such as galvinoxyl,[3] TMPD-ClO_4,[4] CA-K,[5] TCNQ-M (M=Na, K, Rb),[6] etc., make spin Peierls-like phase transitons between a paramagnetic regular-stack structure and a diamagnetic dimerized structure.

The heterocyclic thiazyl radicals are materials located on the boarderline between organic and inorganic.[7] It is characteristic of this radical family to possess chemical stabilities and strong intermolecular interactions. Their crystals consist of face-to-face π overlaps and side-by-side S···N and S···S contacts similar to those in the interchain arrangements of the inorganic polymer, $(SN)_x$.[8,9] Various interesting physical properties have been reported so far. The neutral radical p-NC-(C_6F_4)-(CN_2S_2) exhibits weak ferromagnetism with a rather high critical temperature of 35.5 K.[10] The cation radical salts 1,3- and 1,4-[$(S_2N_2C)C_6H_4(CN_2S_2)$][X] (X=I, Br) show semimetallic behavior and metal-insulator transitions.[11] N-[(Dichlorophenyl)thio]-2,4,6-triarylphenylaminyl is reported to possess a ferromagnetic intermolecular interaction of $J/k_B = 14$ K.[12] Benzo(bis-1,3,2-dithiazolyl) is a stable biradical whose electron paramagnetic resonance (EPR) spectra are a subject of controversy.[13–15] It is also interesting that unusual phase transitions associated with drastic changes in magnetism were observed in the thiazyl radicals.[16–19]

One of the derivatives, 1,3,5-trithia-2,4,6-triazapentalenyl (TTTA), was prepared by Wolmershäuser and Johann in 1989.[20] Recently we discovered a first-order phase transition in TTTA that occurs with a drastic change in magnetism and with a wide thermal hysteresis loop in the vicinity of room temperature.[21] In this paper we will describe the results of static magnetic measurements, EPR measurements, structural analyses, differential scanning calorimetry (DSC) measurements, and reflection spectroscopy. Based on these, we will discuss the phase transition and the room-temperature magnetic bistability in TTTA.

TABLE I. Crystallographic data for the HT and LT phases of TTTA.

Phase	HT	LT
Crystal size/mm	0.40×0.30×0.30	0.35×0.25×0.22
Crystal system	monoclinic	triclinic
Space group	$P2_1/c$	$P\bar{1}$
a/Å	9.4420(7)	7.5310(5)
b/Å	3.7110(2)	10.0230(8)
c/Å	15.062(1)	7.0240(4)
α/deg		100.598(4)
β/deg	104.630(3)	96.978(5)
γ/deg		77.638(3)
V/Å^3	510.6(1)	507.2(1)
Z	4	2
μ/mm^{-1}	1.315	1.324
$R(F)$, $wR(F)$	0.025, 0.065	0.026, 0.047

II. EXPERIMENTS

TTTA was prepared by a modification of the literature method described in Ref. 19. The single crystals in the shape of a hexagonal prism were obtained by vacuum sublimation. The x-ray diffraction data collections were performed at room temperature with graphite-monochromated Mo $K\alpha$ radiation on a Mac Science DIP-3200 imaging plate system. The absorption correction was applied by integration using the crystal shape. The crystallographic data are summarized in Table I. The structures were solved by a direct method (SIR92). A full-matrix least-squares technique with anisotropic thermal parameters was employed for the structure refinements. The coordinates and the isotropic thermal parameters for the high-temperature (HT) and low-temperature (LT) phases are listed in Tables II and III, respectively. The static magnetic measurements were carried out on a Quantum Design MPMS-*XL* superconducting quantum interference device (SQUID) susceptometer. The diamagnetic correction was performed using a diamagnetic susceptibility that was evaluated by assuming that TTTA was in a nonmagnetic state in the range 100–150 K. The EPR was recorded on a JES RE2X spectrometer equipped with an Oxford He-gas-flow cryostat. The DSC measurements were performed on a Mettler Toledo DSC 822e/200 calorimeter. The polarized reflection spectra were taken at room temperature by using a specially designed spectrometer with a 25 cm grating monochromator (JASCO M25-GT) and an optical microscope. This spectrometer has a halogen lamp and a Xe lamp as light sources, and Si and Ge photodiodes and a photomultiplier as detectors. Suitable light sources and detectors were selected, depending on the energy region. We checked the quality of the sample surface after the measurements and found no damage caused by irradiation.

TABLE II. Fractional coordinates and isotropic thermal parameters for the HT phase of TTTA.

Atom	x	y	z	U_{eq}
C(1)	0.8176(2)	0.3862(6)	0.1271(1)	0.031(1)
C(2)	0.6753(2)	0.2488(7)	0.0850(2)	0.031(1)
N(3)	0.6847(2)	0.3209(7)	0.2555(1)	0.044(1)
N(4)	0.6513(2)	0.1948(6)	−0.0039(1)	0.038(1)
N(5)	0.9019(2)	0.4370(6)	0.0705(1)	0.036(1)
S(6)	0.56636(6)	0.1825(2)	0.16057(4)	0.0436(3)
S(7)	0.84730(7)	0.4536(2)	0.24446(4)	0.0409(3)
S(8)	0.80261(6)	0.3164(2)	−0.03182(4)	0.0377(3)

TABLE III. Fractional coordinates and isotropic thermal parameters for the LT phase of TTTA.

Atom	x	y	z	U_{eq}
S(1)	0.70703(9)	0.03181(7)	−0.3126(1)	0.0301(3)
S(2)	0.54730(9)	0.30665(7)	−0.3544(1)	0.0285(3)
S(3)	1.10239(9)	0.26744(7)	−0.2366(1)	0.0326(3)
S(4)	0.48052(9)	0.37580(6)	0.1218(1)	0.0285(3)
S(5)	0.64288(9)	0.09939(6)	0.1524(1)	0.0293(3)
S(6)	1.03323(9)	0.34112(7)	0.2595(1)	0.0315(3)
N(7)	0.5203(3)	0.1472(2)	−0.3538(4)	0.034(1)
N(8)	0.8989(3)	0.3627(2)	−0.2825(4)	0.029(1)
N(9)	1.0424(3)	0.1174(2)	−0.2472(4)	0.031(1)
N(10)	0.4558(3)	0.2143(2)	0.1098(4)	0.034(1)
N(11)	0.8297(3)	0.4361(2)	0.2152(4)	0.029(1)
N(12)	0.9748(3)	0.1896(2)	0.2407(4)	0.031(1)
C(13)	0.8640(3)	0.1392(3)	−0.2850(4)	0.024(1)
C(14)	0.7822(3)	0.2791(3)	−0.3059(4)	0.024(1)
C(15)	0.7971(3)	0.2101(3)	0.1988(4)	0.023(1)
C(16)	0.7141(3)	0.3507(3)	0.1838(4)	0.023(1)

III. EXPERIMENTAL RESULTS

A. Room-temperature magnetic bistability

The temperature dependence of the paramagnetic susceptibilities χ_p for a polycrystalline sample of TTTA was examined in the range 1.8–370 K. The results are depicted in Fig. 1(a). The bold arrow in this figure indicates the value of χ_p for the virgin sample just after the sublimation. As the sample is cooled from room temperature, χ_p shows a slight decrease (open circles). At 230 K, χ_p begins to quickly decrease, becoming zero at 170 K. Below 100 K the plots of χ_p show a gradual increase, caused by the Curie spins on lattice defects. The presence of paramagnetic lattice defects is also demonstrated by means of EPR, as shown later. It is considered that TTTA is intrinsically diamagnetic at low temperatures. When the sample is heated from the lowest temperature, χ_p gradually decreases and becomes almost zero over the range of 80–300 K (open triangles). Above 120 K, χ_p shows a very slight increase with a small step at 180 K, as shown in the inset of Fig. 1(a).[22] We experienced that the samples of worse crystallinity exhibited an enhancement to this step, together with an increase of the Curie lattice defects in number. The relation between the Curie lattice defects and the anomaly at 180 K is interesting, because it could be a key to an understanding of the phase transition in TTTA, but it is hard to rationalize it now. At 305 K, χ_p

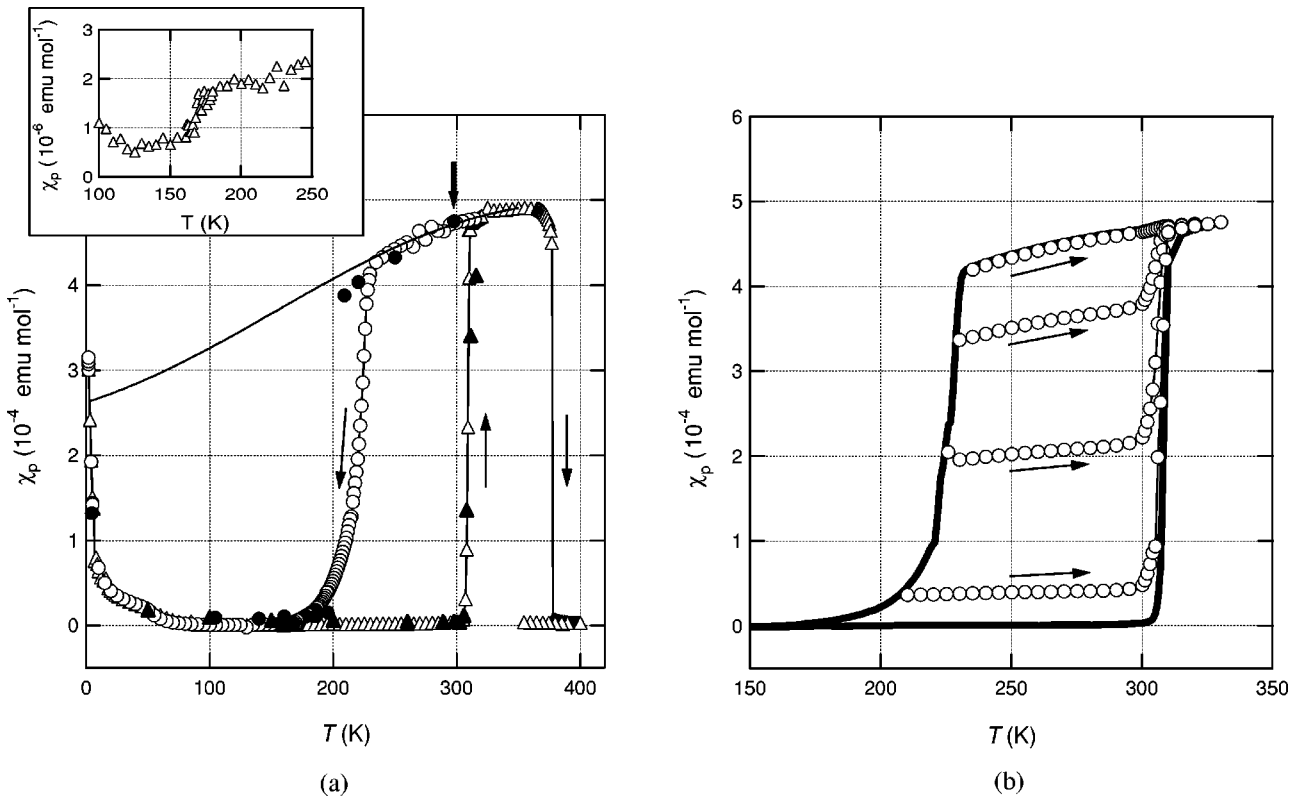

FIG. 1. (a) The temperature dependence of the paramagnetic susceptibility χ_p for a polycrystalline sample of TTTA on cooling (open circles) and on heating (open triangles). The inset depicts the result on heating in the range 100–250 K in an enlarged scale. The bold arrow indicates the χ_p value for the virgin sample just after sublimation. The solid curve is the theoretical best fit of Eq. (1) with $J/k_B = -320$ K and $zJ'/k_B = -360$ K. The solid circles and triangles represent the EPR spin susceptibility χ_{EPR} on cooling and heating, respectively. (b) The magnetic responses of TTTA to heating for the samples at $T_{c\downarrow}$ with different starting points. The bold gray curves depict the hysteresis loop shown in Fig. 1(a).

shows a sudden increase to a value which is almost the same as the initial one. Above 365 K, TTTA exhibits an irreversible transition to a diamagnetic state caused by chemical decomposition. The magnetic measurements indicate a first-order phase transition with a surprisingly wide hysteresis loop: $T_{c\downarrow} = 230$ K and $T_{c\uparrow} = 305$ K.[23] Since this loop includes the room temperature (290 K), the material exhibits a magnetic bistability at room temperature.

To make sure of the hysteresis loop, we performed the following experiments. On the SQUID susceptometer, we slowly cooled the HT phase and stopped the cooling just during the phase transition to the diamagnetic LT phase. Then we gradually raised the sample temperature, following the magnetic response. The results of four runs with different starting points are depicted in Fig. 1(b). In every run the plots of χ_p clearly indicate that there is little change in the ratio between the HT and LT phases in the temperature range within the loop. This means that the two phases can stably coexist in this range. The hysteresis is intrinsic at least in the time scale of the laboratory.

B. Structural change at phase transition

The HT and LT phases were isolated by annealing the material at 40 °C and at liquid nitrogen temperature for several hours, respectively. Their crystal structures were studied at room temperature. We have briefly described the structures of the two phases in a previous report,[21] although the lattice parameters included rather large deviations, probably because of the mosaic character of the examined crystal. To improve the reliability, we reexamined the structures of the two phases in this study.

The HT phase crystallizes in the monoclinic $P2_1/c$ space group, where one molecule is crystallographically independent. This structure is identical to the one reported in Ref. 19. On the other hand, the LT phase crystallizes into the triclinic $P\bar{1}$ space group, where two molecules are independent. The cell volume of the LT phase is smaller than that of the HT phase by 3.4 $Å^3$. There is no significant difference among the molecular structures in the two phases. The atom numbering scheme is shown in Fig. 2, where the distributions of the atomic charges and the spin densities, calculated by using the semiempirical molecular orbital calculations (PM3/UHF),[24] are also presented. The calculations clearly demonstrate the fairly localized spin densities on the -S-N-S- moiety and the strong, electric polarization.

Figure 3(a) depicts the projections of the structure of the HT phase along the *b* and *c* axes. The structure of the HT phase consists of a polar 1D stacking column along the *b* axis with strong intercolumn interactions. In the column, the molecules are related by translational relations, having a con-

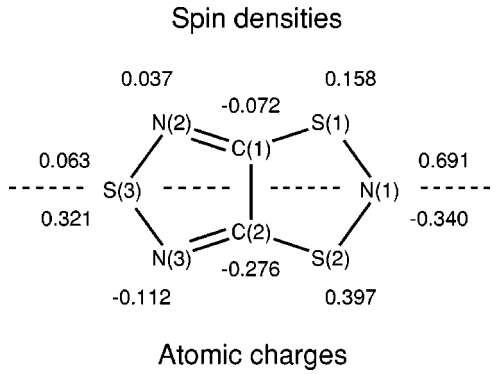

FIG. 2. The atom numbering scheme and the distributions of the atomic charges and the spin densities.

stant interval. The overlap between the neighboring molecules is slightly shifted. One column is surrounded by six neighbors with short S···N and S···S contacts. The dashed lines in Fig. 3(a) indicate the distances, which are shorter than the sums of the van der Waals radii in the intercolumn.

TABLE IV. Calculated overlap integrals ($\times 10^{-3}$) in the HT and LT phases.

HT		LT	
p	-7.5	p_1	-58.3
		p_2	-21.7
q_1	-11.5	q_1	3.9
q_2	5.2	q_2	-2.2
q_3	-6.8	q_3	-6.9
q_4	3.5	q_4	-2.7
q_5	-2.4	q_5	-0.3
q_6	-3.0	q_6	-0.1
		q_7	-2.2

We calculated the intermolecular overlap integrals with the singly-occupied molecular orbital (SOMO) obtained by the extended Hückel method.[25] The results are shown in Table IV. The intracolumn overlap integral p is large, be-

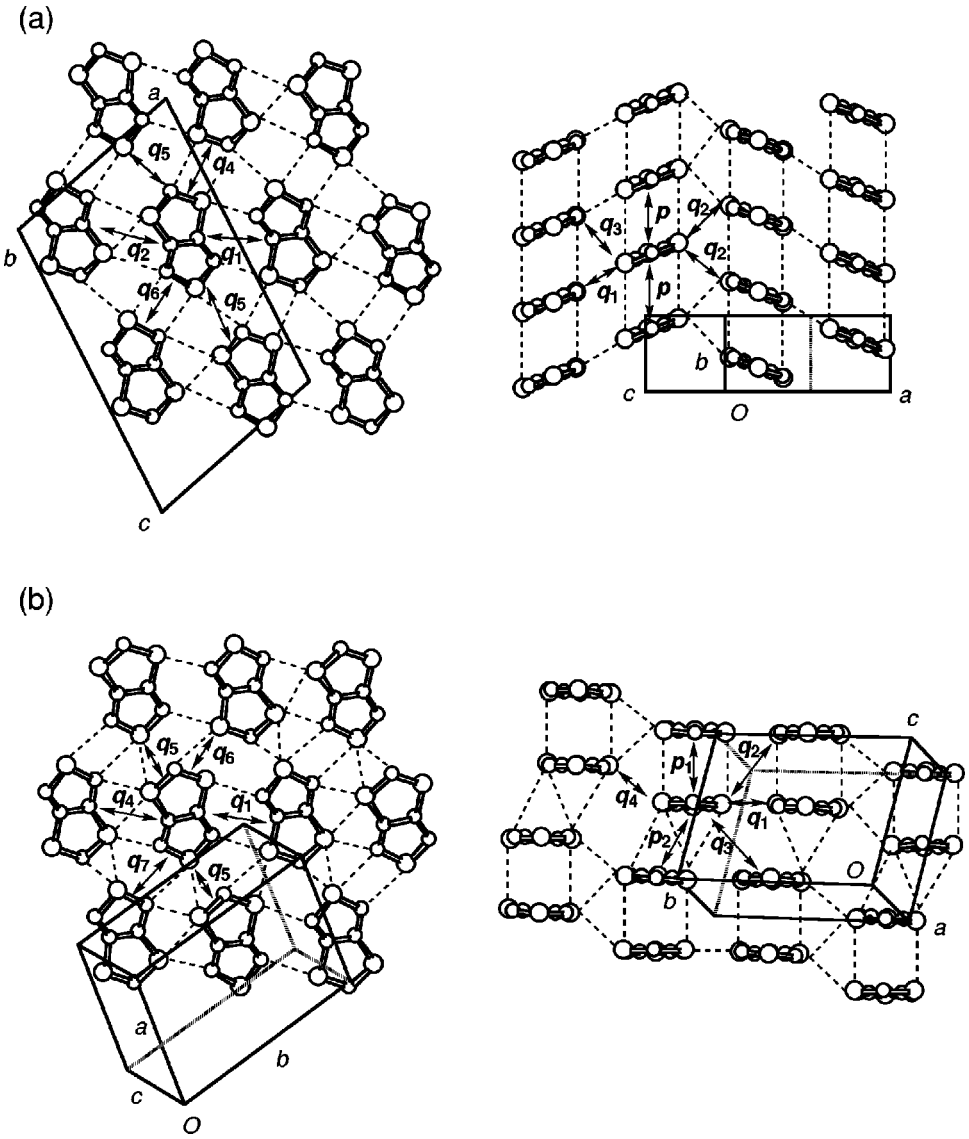

FIG. 3. The projections of the crystal structures of TTTA for the HT phase (a) and the LT phase (b). The labels p_i and q_j are for the overlap integrals shown in Table IV.

cause the polar stacking column includes a short contact between the -S-N-S- moieties on which the SOMO's are concentrated. However, the largest overlap integral is q_1, probably due to the short N(2)$\cdots$S(1) contact [3.128(2) Å]. The overlaps p and q_1 bring about a ladder-type interaction in the structure of the HT phase. The other overlap integrals q_2–q_6 are smaller than p or q_1, but the differences among them are not significant. The reflection spectra described later are consistent with these calculations; they indicate the charge-transfer interactions both parallel and perpendicular to the stacking direction.

The HT phase has a multidimensional network, so that it is difficult to select a magnetic model to analyze the magnetic data. In addition, the magnetic data for this phase are limited to the temperature range 230–365 K. Then, to roughly estimate the magnetic interactions in the HT phase, we interpreted the magnetic behavior of the HT phase by the model of 1D antiferromagnetic chains, modified by the addition of a mean-field correlation to account for the intercolumn interactions,[26] namely, by

$$\chi_{\mathrm{p}}=\frac{\chi'}{1-(2zJ'/Ng^2\mu_{\mathrm{B}}^2)\chi'}, \tag{1}$$

in which

$$\chi'=\frac{Ng^2\mu_{\mathrm{B}}^2}{k_{\mathrm{B}}T}\frac{A+Bx+Cx^2}{1+Dx+Ex^2+Fx^3}, \tag{2}$$

with

$$x=\frac{|J|}{k_{\mathrm{B}}T}, \tag{3}$$

where J and J' are the intracolumn and intercolumn magnetic coupling constants, respectively, z is the number of nearest neighbors, k_{B} is the Boltzmann constant, and μ_{B} is the Bohr magneton. The constants A–F are defined elsewhere.[26] The solid curve in Fig. 1(a) is the theoretical best fit with the parameters $J/k_{\mathrm{B}}=-320$ K and $zJ'/k_{\mathrm{B}}=-360$ K ($z=6$). Although the theoretical curve reproduces well the observed behavior, the obtained values for J and J' suggest that the 1D model is fairly inadequate and 3D effects are compatible in strength.

The structure of the LT phase is depicted in Fig. 3(b), where the two crystallographically independent molecules are denoted by *A* and *B*. The molecular packing is crucially different from that in the HT phase. The molecular planes are almost parallel in the LT phase, while the unit cell of the HT phase includes two molecular-plane orientations. In addition, TTTA molecules are strongly dimerized in the LT phase along the stacking direction with an eclipsed overlap between the molecular planes. Exactly speaking, the molecular planes are not parallel in the intradimer arrangement; the distance between the -S-N-S- moieties is shorter by ~0.2 Å than that between the -N-S-N- moieties, probably reflecting a bonding interaction between the unpaired electrons concentrated on the -S-N-S- moieties. This suggests that the bonding formation would be a driving force of the phase transition. In the interdimer arrangements, there are many intermolecular and interatomic distances shorter than the sums of the van der Waals radii.

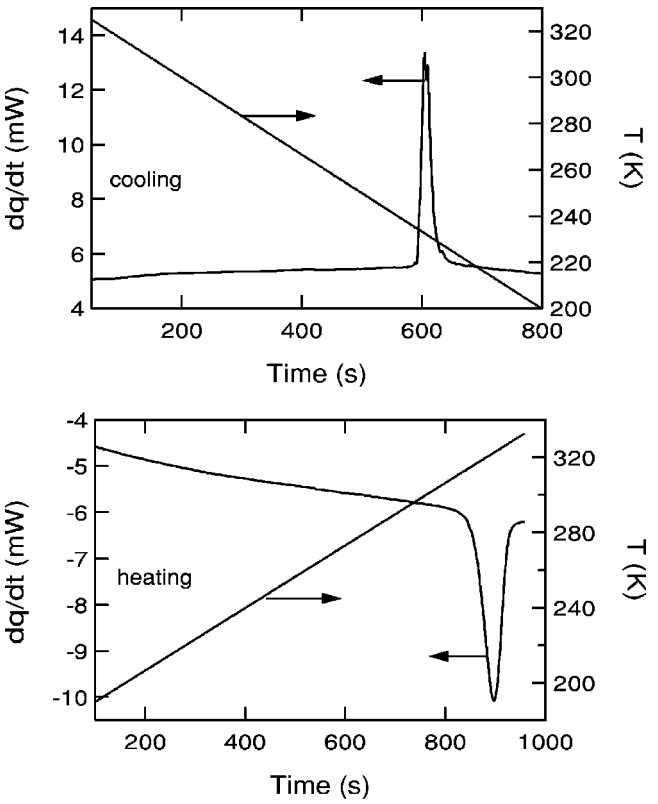

FIG. 4. The DSC curves for TTTA upon cooling (a) and heating (b).

Table IV shows the calculated overlap integrals in the LT phase. The intradimer overlap integral p_1 is so large that the formation of a singlet radical dimer would cause the diamagnetic property of the LT phase. The interdimer overlap integral p_2 in the stacking direction is unexpectedly intensified compared with the p value in the HT phase. The intercolumn interactions, represented by q_1–q_7, are much smaller than p_1 or p_2 in the LT phase. The calculated overlap integrals suggest that the phase transition in TTTA results in an enhancement of anisotropy in interaction in the LT phase. We analyze the slight increase in χ_{p} above 200 K for the LT phase with the Bleaney-Bowers equation.[27] The intradimer exchange coupling constant, which is half of the spin gap, is roughly estimated to be $J/k_{\mathrm{B}}=-650$ K. This is much larger than the J value in the HT phase.

C. Thermal properties

The phase transition of TTTA was examined by means of DSC. The results are shown in Fig. 4. In the cooling and heating processes, we found an exothermic and an endothermic transition at 234 and 315 K (onset temperatures), respectively. The thermal hysteresis is confirmed in this measurement. The transition enthalpies ΔH at $T_{c\downarrow}$ and $T_{c\uparrow}$ are obtained to be 2210 and 2340 J mol^{-1}, respectively. The difference is probably due to the fact that the HT and LT phases have different heat capacities. The transition entropies

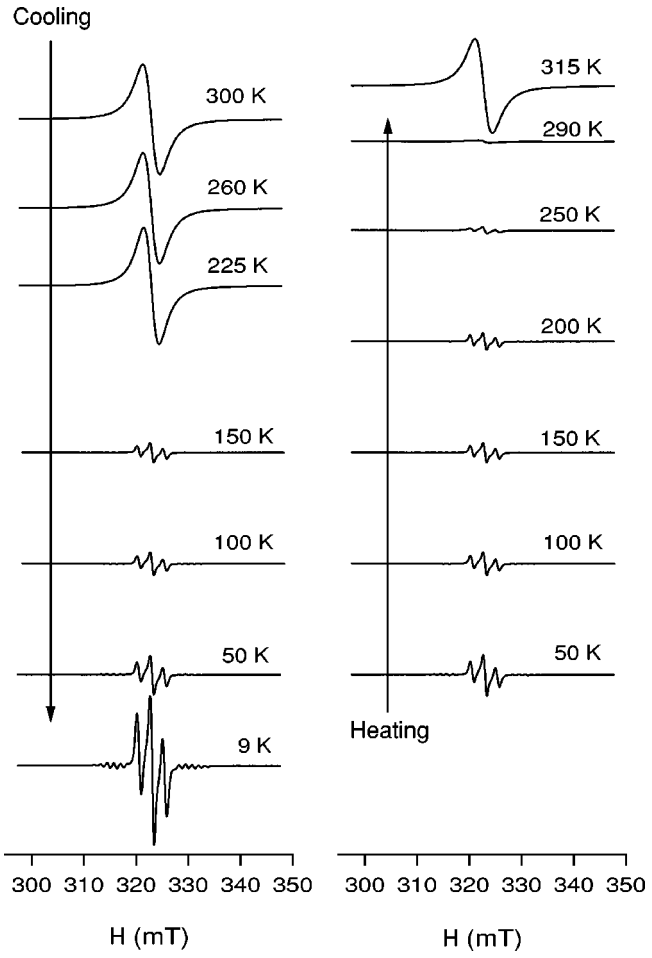

FIG. 5. The *X*-band EPR spectra of TTTA at the representative temperatures.

ΔS are estimated as $\Delta S_{\downarrow}=\Delta H_{\downarrow}/T_{c\downarrow}=9.44$ J K^{-1} mol^{-1} and $\Delta S_{\uparrow}=\Delta H_{\uparrow}/T_{c\uparrow}=7.43$ J K^{-1} mol^{-1} upon cooling and heating, respectively. The maximum estimation of the magnetic contribution is $R\ln 2(=5.76$ J K^{-1} mol$^{-1})$. Since the HT phase involves strong antiferromagnetic interactions, the real contribution would be much smaller than $R\ln 2$. In spite of this, the observed transition entropies are larger than $R\ln 2$. Cooperation of the lattice system is suggested in the phase transition of TTTA. The presence of such excess entropy is similar to those in the spin crossover transitions[28] and in the first-order phase transitions of the quasi-1D molecule-based magnetic materials.[29–31]

D. EPR and lattice defects

We examined the temperature dependence of *X*-band EPR on a single crystal of TTTA. The crystal was fixed with Araldite glue,[32] as the crystallographic *b* axis of the HT phase became parallel to the magnetic field. The EPR susceptibilities χ_{EPR} were obtained by integrating the EPR lines. The derivatives of the EPR lines at representative temperatures are depicted in Fig. 5. The temperature dependence of χ_{EPR} is compared with that of χ_{p} in Fig. 1, where the values of χ_{EPR} are normalized on the assumption that $\chi_{\mathrm{EPR}}=\chi_{\mathrm{p}}$ in the HT phase. The dependence of χ_{EPR} well agrees with that of χ_{p}. The top, left signal in Fig. 5 shows the resonance for the HT phase at 300 K. The angular dependence of the g factor and the peak-to-peak linewidth ΔH_{pp} for this HT phase signal were studied at 300 K. The principal g factors were determined to be $g_1=2.0094$, $g_2=2.0028$, and $g_3=2.0009$ ($\bar{g}=2.0043$). They were typical for the thiazyl radicals. We also examined the angular dependence of ΔH_{pp}. There were no minima at the magic angles, suggesting 3D dipole-dipole and/or exchange interactions, which were consistent with the crystal structure of the HT phase and with the results of the static magnetic measurements.

When the sample is cooled, the phase transition is found at $\sim$200 K in the EPR measurements. Below 200 K, complicated patterns appear as shown in Fig. 5. They are caused by paramagnetic lattice defects. The angular dependence of the strong three lines (not shown) indicates that they are hyperfine structures of ^{14}N with a coupling constant $a_{\mathrm{N}(1)}$ of 1.2 mT. This value agrees well with the reported one.[33] The signal at 9 K clearly indicates the satellite signals near 315 and 330 Oe. They are probably the hyperfine signals of ^{33}S whose natural abundance is 0.76%. The observation of these hyperfine structures indicates that the paramagnetic lattice defects are well isolated in the diamagnetic lattice of the LT phase. They are supposed to be radical monomers after the dimerization.

In the heating process, the phase transition occurs above 300 K. The magnetic bistability of TTTA is further confirmed by means of EPR. Since EPR is highly sensitive to the spin state of organic radicals, the two phases of TTTA can be easily distinguished by EPR rather than SQUID measurements.

We carefully looked for fine structures of triplet excitons in the LT phase in the temperature range 100–300 K, because this phase consisted of the radical dimers, but we could not find them. The absence of the triplet exciton would be caused by the interdimer interactions in the LT phase.

E. Optical properties

It is worth mentioning the color changes at the phase transition. The HT phase is dark purple, while the LT phase is dark green. This thermochromism is due to a change in the optical properties at the phase transition. To clarify the electronic transitions responsible for the observed color change, we examined the polarized reflection spectra on the (100) surface of the HT phase and on the (010) surface of the LT phase at room temperature. They are the same surface of the hexagonal prism of the TTTA crystal. The reflectivity R spectra are presented in Fig. 6, in which the solid and dotted curves show the results with the electric vector $\boldsymbol{E}$ of the lights parallel ($E_{\parallel}$) and perpendicular ($E_{\perp}$) to the π-stacking axis, respectively. The small peaks at 3.2 eV for the HT phase appearing in both polarizations cause the purple color of this phase, while the strong band for the LT phase at 2.2 eV in the $E_{\parallel}$ spectrum makes this phase green.

The obtained reflectivity R spectra were converted to the optical conductivity σ spectra by using the Kramers-Kronig relation. The energy region of the R data was limited to

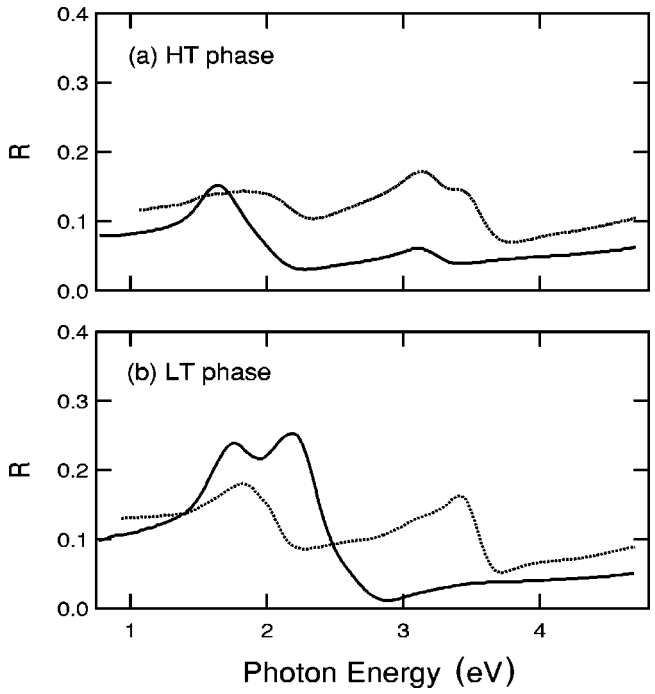

FIG. 6. The polarized reflectivity R spectra for the HT (a) and LT phases (b). The solid and the dotted curves show the result under the polarization parallel ($E_{\|}$) and perpendicular ($E_{\perp}$) to the π stacking axis, respectively.

0.8–4.9 eV, so that the Roessler correction was employed in the transformation.[34] Hereafter we will discuss the electronic transitions of TTTA in the σ spectra shown in Fig. 7. Both the HT and LT phases exhibit strong bands around 3–4 eV,

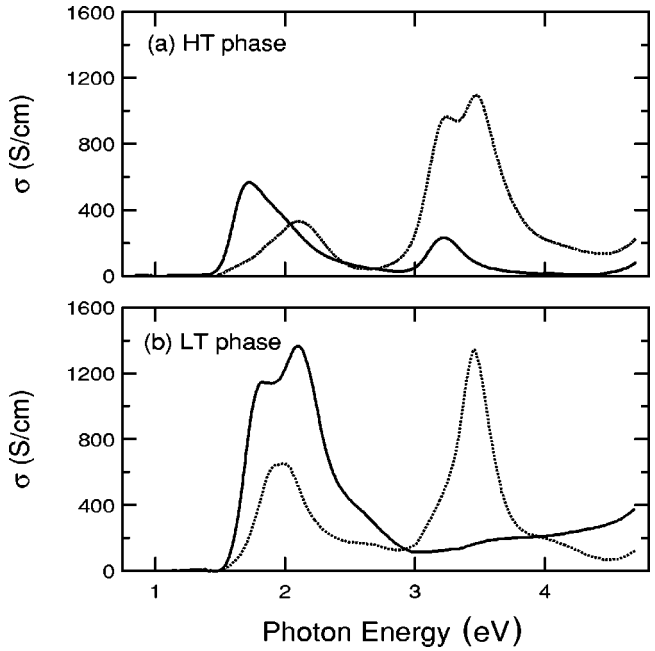

FIG. 7. The optical conductivity σ spectra for the HT (a) and LT (b) phases. The solid and the dotted curves show the result under the polarization parallel ($E_{\|}$) and perpendicular ($E_{\perp}$) to the π stacking axis, respectively.

predominantly polarized for $E_{\perp}$. Since this direction of $\boldsymbol{E}$ is nearly parallel to the long axis of TTTA, these bands can be assigned to intramolecular π-π transitions. The bands observed below 2.5 eV are assignable to the charge-transfer (CT) bands. The energy of the CT band is a crude measure for the on-site Coulomb repulsion energy U on the TTTA molecule; the value of U is roughly evaluated to be 2 eV. Such a large value of U is considered to reflect the small molecular structure of TTTA. There is a crucial difference between the CT bands in the two phases. The HT phase exhibits peak structures at 1.75 eV for $E_{\|}$ and 2.1 eV for $E_{\perp}$ [Fig. 7(a)]. We can attribute the peaks for $E_{\|}$ and $E_{\perp}$ to the intra- and intercolumn CT transitions, respectively, judging from their polarization dependence. The intra- and intercolumn CT's are related to the overlap integrals p and q_1–q_6, respectively. The largest one among q_1–q_6 is q_1 so that it would dominate the intercolumn CT observed for $E_{\perp}$. Although the absolute value of q_1 (11.5×10^{-3}) is larger than that of p (7.5×10^{-3}), the intensity of the CT band for $E_{\perp}$ is slightly smaller than that for $E_{\|}$. The dipole moment of the intercolumn CT represented by q_1 is not parallel to the (100) surface. This probably decreases the observed transition intensity. In addition, this dipole moment has a finite component for $E_{\|}$. In fact, there is a hump structure around 2.1 eV in the spectrum for $E_{\|}$, which we extrapolate has the same origin as the peak for $E_{\perp}$. On the other hand, the dipole moment of the intracolumn CT represented by p is parallel to the (100) surface and has only a component for $E_{\|}$. As a result, the observed intensity of the CT band for $E_{\perp}$ is not so enhanced as compared with that for $E_{\|}$. Taking account of these situations, we can consider that the intra- and intercolumn CT interactions are comparable to each other. The multidimensional interactions in the HT phase suggested in the magnetic measurements are supported by optical spectroscopy.

After the phase transition to the LT phase, the CT band shows a drastic change, as seen in Fig. 7(b). In the $E_{\|}$ spectrum, it splits into two bands with a large intensity enhancement. In contrast the CT band for $E_{\perp}$ is only slightly intensified. It is characteristic of the LT phase that the intensity of the CT band depends strongly on the polarization: the intensity for $E_{\|}$ is much larger than that for $E_{\perp}$. This is also consistent with the results of the intermolecular overlap integral calculations, which suggest a strong enhancement of anisotropy in the LT phase. The split of the CT band for $E_{\|}$ is probably caused by the alternation: the two bands at 1.8 and 2.1 eV in Fig. 7(b) can be ascribed to the interactions represented by p_2 and p_1, respectively, based on their intensities. The structure around 2 eV for $E_{\perp}$ seems to be composed of at least two bands, which would be related to the intercolumn CT transitions represented by q_1–q_7. By comparing the polarization dependence of the intensity in the two phases, we can reasonably conclude that the dimensionality of the LT phase is decreased as compared with the HT phase.

IV. DISCUSSION

In the previous section we described the room-temperature magnetic bistability in TTTA that is caused by

the first-order phase transition. Generally speaking, it is not easy to clear up the causes of the first-order phase transitions, but it is not very difficult to qualitatively understand them based on a case-by-case discussion. In our previous paper we suggested incorporation of the spin-Peierls instability, because we observed a strong alternation along the stacking direction in the LT phase. Actually the overlap-integral calculations and the optical spectra indicate an enhancement of 1D character in the LT phase. If the structure of the HT phase involves instability toward the 1D lattice, this would couple with the spin-Peierls instability, resulting in lattice alternation. However, the calculations also indicate that both intracolumn overlap integrals p_1 and p_2 in the LT phase are larger than the intracolumn overlap p in the HT phase. This does not agree with the picture of the spin-Peierls transition in which the centers of gravity in the dimers do not move: enhancement of the intradimer interaction automatically means decrease of the interdimer interaction in intensity for the 1D column. It is natural to conclude that the phase transition in TTTA is predominantly structural in character, and the spin-Peierls instability may play a secondary role assisting the transition, as discussed for Rb-TCNQ.[35]

It is also important to discuss the causes of the large hysteresis loop. It is notable that the HT phase consists of intra- and intercolumn interactions. In the field of molecular magnetism, spectacular examples of molecular bistability include the specific Fe(II) spin-crossover complexes, in which the transitions occur with wide thermal hysteresis in the vicinity of room temperature.[36] As the Fe(II) sites are bridged by ligands in such specific complexes, it is believed that intersite interactions bring about the hysteresis.[37] The strong intercolumn interactions in TTTA possibly cooperate with the spin-Peierls instability and result in the first-order phase transition. Another possible cause can be seen in the nearest-neighboring intermolecular arrangements. While the two molecules exhibit a slipped overlap along the shorter molecular axis in the HT phase, the two molecules are completely eclipsed in the LT phase.[21] The geometry in the LT phase maximizes the exchange energy, because of the overlap between the molecular orbitals of the unpaired electrons, but it suffers electrostatic repulsion caused by encounters of the polarized charges of the same sign. It is considered that the gain in exchange energy overcomes the loss in electrostatic energy in this phase and the structure of the HT phase is obtained by a balance between the two kinds of energies. The competition between the exchange and electrostatic energies in the dimer may make a potential barrier between the structures of the LT and HT phases and result in the hysteresis loop.

We suggested two possible reasons for the large hysteresis: the intercolumn interactions and the competition between exchange and electrostatic energies. It is worth noting that the intercolumn interactions are caused mainly by the S···N electrostatic interactions. Therefore we believe that the electrostatic interactions, which are characteristic of thiazyl radicals, would play a crucial role in the realizaion of the hysteresis loop.

V. CONCLUSION

We studied the room-temperature magnetic bistability in TTTA that was realized by the first-order phase transition between the paramagnetic HT phase and the diamagnetic LT phase. The EPR and DSC measurements confirmed the presence of the wide hysteresis loop associated with the transition. Since EPR was very sensitive to the spin states of organic radicals, the two phases were more easily distinguished by means of EPR rather than SQUID. The polarized reflection spectra and the intermolecular overlap-integral calculations indicated the multidimensional CT interactions in the two phases, while the anisotropy was enhanced in the LT phase. It was suggested that the phase transition of TTTA would be governed by structural factors, such as molecular packing, electrostatic interactions, etc., rather than the spin-Peierls mechanism.

ACKNOWLEDGMENTS

The authors would like to thank Michio Sorai, Kazuya Saito, Masao Ogata, Yoshio Teki, Akiko Nakao, Tatsuro Imakubo, and Tokutaro Komatsu for their helpful discussions. The authors are also indebted to Yasushi Ikeda and Chitoshi Saeki of Mettler-Toledo K. K. for the measurements of the DSC data. This work was supported by a Grant-in-Aid for Scientific Research from the Ministry of Education, Science, and Culture, Japanese government.

[1] *Magnetism: A Supramolecular Function*, Vol. 484 of *NATO Advanced Study Institute, Series C*, edited by O. Kahn (Kluwer Academic, Dordrecht, 1995); *Supramolecular Engineering of Synthetic Metallic Materials*, Vol. 518 of *NATO Advanced Study Institute, Series C*, edited by J. Veciana, C. Rovira, and D. B. Amabilino (Kluwer Academic, Dordrecht, 1998); *Organic Superconductors*, 2nd ed., edited by T. Ishiguro, K. Yamaji, and G. Saito (Springer-Verlag, Borlin, 1998); *Magnetic Properties of Organic Materials*, edited by P. M. Lahti (Marcel Dekker, New York, 1999).

[2] H.A. Goodwin, Coord. Chem. Rev. **18**, 293 (1976); P. Gutlich, Struct. Bonding (Berlin) **44**, 83 (1981); E. Konig, G. Rotter, and S.K. Kulshreshtha, Chem. Rev. **85**, 219 (1985); J.K. Beattie, Adv. Inorg. Chem. **32**, 1 (1988); P. Gurtlich and A. Hauser, Coord. Chem. Rev. **97**, 1 (1990).

[3] K. Mukai, Bull. Chem. Soc. Jpn. **42**, 40 (1969); K. Awaga, T. Sugano, and M. Kinoshita, Chem. Phys. Lett. **128**, 587 (1986).

[4] N. Elliot and M. Wolfsberg, Phys. Rev. **91**, 435 (1955); W. Duffy, Jr., J. Chem. Phys. **36**, 490 (1962); J.L. de Boer and A. Vos, Acta Crystallogr., Sect. B: Struct. Crystallogr. Cryst. Chem. **28**, 835 (1972).

[5] J.J. André, J. Clémentz, R. Jesser, and G. Weill, C. R. Seances Acad. Sci., Ser. B **266**, 1057 (1968); T. Sugano, T. Ohta, and H. Kuroda, Chem. Phys. Lett. **34**, 164 (1975).

[6] J.G. Vegter, T. Hibma, and J. Kommandeur, Chem. Phys. Lett. **3**, 427 (1969); N. Sakai, I. Shirotani, and S. Minomura, Bull. Chem. Soc. Jpn. **45**, 3321 (1972); M. Konno and Y. Saito, Acta Crystallogr., Sect. B: Struct. Crystallogr. Cryst. Chem. **30**, 1294 (1974); **31**, 2007 (1975); M. Konno, T. Ishii, and Y. Saito, *ibid.* **33**, 763 (1977).

[7] R.T. Oakley, Prog. Inorg. Chem. **36**, 299 (1988); J.M. Rawson, A.J. Banister, and I. Lavender, Adv. Heterocycl. Chem. **62**, 137 (1995); J.M. Rawson and G.D. McManus, Coord. Chem. Rev. **189**, 135 (1999).

[8] M. Boudelle and P. Michel, Acta Crystallogr., Sect. A: Cryst. Phys., Diffr., Theor. Gen. Crystallogr. **28**, S199 (1972).

[9] M.J. Cohen, A.F. Garito, A.J. Heeger, A.G. MacDiarmid, C.M. Mikulski, M.S. Saran, and J. Kleppinger, J. Am. Chem. Soc. **98**, 3844 (1976).

[10] A.J. Banister, N. Bricklebank, I. Lavender, J.M. Rawson, C.I. Gregory, B.K. Tanner, W. Clegg, M.R. Elsegood, and F. Palacio, Angew. Chem. Int. Ed. Engl. **35**, 2533 (1996); F. Palacio, G. Antorrena, M. Castro, R. Burriel, J.M. Rawson, J.N.B. Smith, N. Bricklebank, J. Novoa, and C. Ritter, Phys. Rev. Lett. **79**, 2336 (1997).

[11] C.D. Bryan, A.W. Cordes, R.M. Fleming, N.A. George, S.H. Glarum, R.C. Haddon, R.T. Oakley, T.T. Palstra, A.S. Perel, L.F. Schneemeyer, and J.V. Waszczak, Nature (London) **365**, 821 (1993); C.D. Bryan, A.W. Cordes, R.M. Fleming, N.A. George, S.H. Glarum, R.C. Haddon, C.D. MacKinnon, R.T. Oakley, T.T. Palstra, and A.S. Perel, J. Am. Chem. Soc. **117**, 6880 (1994).

[12] Y. Teki, K. Itoh, A. Okada, H. Yamakage, T. Kobayashi, K. Amaya, S. Kurokawa, S. Ueno, and Y. Miura, Chem. Phys. Lett. **270**, 573 (1997).

[13] T.M. Barclay, A.W. Cordes, R.H. de Laat, J.D. Goddard, R.C. Haddon, J.D. Jeter, R.C. Mawhinney, R.T. Oakley, T.M.M. Palstra, G.W. Patenaude, R.W. Reed, and N.P.C. Westwood, J. Am. Chem. Soc. **119**, 2633 (1997).

[14] K.A. Williams, M.J. Nowak, E. Dormann, and F. Wudl, Synth. Met. **14**, 233 (1986); N.J. Norwak, K.A. Williams, R.O. Angus, Jr., and F. Wudl, J. Am. Chem. Soc. **109**, 2594 (1987).

[15] G. Wolmershäuser, M. Schnauber, and T. Wilhelm, Synth. Met. **14**, 239 (1986).

[16] E.G. Awere, N. Burford, R.C. Haddon, S. Parsons, J. Passmore, J.V. Waszczak, and P.S. White, Inorg. Chem. **29**, 4821 (1990).

[17] S. Brownridge, H. Du, S.A. Fairfurst, R.C. Haddon, H. Oberhammer, S. Parsons, J. Passmore, M.J. Schriver, L.H. Sutcliffe, and N.P.C. Westwood, J. Chem. Soc. Dalton Trans. **2000**, 3365 (2000).

[18] T.M. Barclay, A.W. Cordes, N.A. George, R.C. Haddon, M.E. Itkis, M.S. Mashuta, R.T. Oakley, G.W. Patenaude, R.W. Reed, J.F. Richardson, and H. Zhang, J. Am. Chem. Soc. **120**, 352 (1998).

[19] T.M. Barclay, A.W. Cordes, N.A. George, R.C. Haddon, M.E. Itkis, and R.T. Oakley, Chem. Commun. (Cambridge) **1999**, 2269 (1999).

[20] G. Wolmershäuser and R. Johann, Angew. Chem. Int. Ed. Engl. **28**, 920 (1989).

[21] W. Fujita and K. Awaga, Science **286**, 261 (1999).

[22] We examined temperature-variable x-ray crystal analyses and EPR measurements, but the anomaly at 180 K was not clearly detected in these measurements.

[23] When the sample was fixed with grease in the SQUID tube, the phase transition sometimes occurred at 320 K. We experienced that the transition temperature depended on the crystallinity, local stress, pressure, etc.

[24] J.J.P. Stewart, QCPE Bull. **10**, 86 (1990).

[25] T. Mori, A. Kobayashi, Y. Sasaki, H. Kobayashi, G. Saito, and H. Inokuchi, Bull. Chem. Soc. Jpn. **57**, 627 (1984).

[26] W.E. Estes, D.P. Gavel, W.E. Hatfield, and D.J. Hodgson, Inorg. Chem. **17**, 1415 (1978).

[27] B. Bleaney and K.D. Bowers, Proc. R. Soc. London, Ser. A **214**, 451 (1952).

[28] M. Sorai and S. Seki, J. Phys. Chem. Solids **35**, 555 (1974).

[29] H. Chihara, M. Nakamura, and S. Seki, Bull. Chem. Soc. Jpn. **38**, 1776 (1965).

[30] K. Kosaki, H. Suga, S. Seki, K. Mukai, and Y. Deguchi, Bull. Chem. Soc. Jpn. **42**, 1525 (1969); K. Awaga, T. Sugano, M. Kinoshita, T. Matsuo, and H. Suga, J. Chem. Phys. **87**, 3062 (1987).

[31] A. Kosaki, M. Sorai, H. Suga, and S. Seki, Bull. Chem. Soc. Jpn. **50**, 810 (1977).

[32] TTTA is ''soluble'' to silicon grease. When the crystals of TTTA are fixed with silicon grease in EPR tubes, the sharp three-line hyperfine structures caused by N(1) spoiled the bulk signal.

[33] Y.-L. Chung, J.P.B. Sandell, L.H. Sutcliffe, H. Joly, K.F. Preson, R. Johann, and G. Wolmershäuser, Magn. Res. Chem. **29**, 625 (1991).

[34] D.M. Roessler, J. Appl. Phys. **16**, 1119 (1965).

[35] H. Okamoto, Y. Tokura, and T. Koda, Phys. Rev. B **36**, 3858 (1987).

[36] J. Kröber, E. Codjvie, O. Kahn, F. Groliere, and C. Jay, J. Am. Chem. Soc. **115**, 9810 (1993).

[37] O. Kahn, *Molecular Magnetism* (VCH, New York, 1993), p. 60.